# Biomimetic Nylon 6-Baghdadite Nanocomposite Scaffold for Bone Tissue Engineering

V. Abbasian, R. Emadi, M. Kharaziha*

Department of Materials Engineering, Isfahan University of Technology, Isfahan 84156-83111, Iran

## ARTICLE INFO

## ABSTRACT

Nature creates soft and hard ingredients revealing outstanding properties by adjusting the ordered assembly of simple primarily components from the nano- to the macro-scale. To simulate the important features of native tissue architecture, wide researches are being performed to develop new biomimetic custom-made composite scaffolds for tissue engineering. Here, we introduced a three-dimensional (3D) biomimetic scaffold based on the cuttlefish bone (CB) as a sacrificial template for bone tissue engineering. By combination of nylon 6 (N6), various amounts of baghdadite (BG) nanopowder and sacrificial template CB, a novel nanocomposite scaffolds was successfully developed with hierarchical microstructure and open pores in the range size in long and minor axis of 153–253 μm and 39–70 μm, respectively, depending on the BG content. In addition, incorporation of BG improved the mechanical properties of the scaffolds. Noticeably, the compressive strength and compressive modulus enhanced from $0.47 \pm 0.05$ to $1.41 \pm 0.25$ MPa and from $3.16 \pm 0.14$ to $6.23 \pm 0.3$ MPa, respectively. Moreover, results demonstrated that the incorporation of BG nanoparticles in the N6 matrix significantly improved bioactivity in simulated body fluid and increased degradation rate of N6 scaffold. Additionally, 3D nanocomposite scaffolds disclosed meaningfully excellent cellular responses. It is envisioned that the provided N6-BG nanocomposite scaffold might be a promising candidate for bone tissue engineering applications.

## 1. Introduction

Bone, as the major component of the human body's skeleton, is an inorganic–organic biocomposite including collagen as the organic and carbonated hydroxyapatite nanoparticles as the inorganic compounds with hierarchical organization in three dimensions [1]. Bone could interface with several injuries including fractures, tumors, osteoporosis and osteonecrosis, which are often associated with pain, disability, high morbidity and mortality [2,3]. Tissue engineering has shown enormous potentials in development of biological alternatives for harvested and damaged tissues [4].The main component of tissue engineering is three dimensional (3D) scaffolds acting as a extracellular matrix for cells to stimulate tissue regeneration [5].

While enormous advancement has been performed to design the scaffolds via conventional approaches including phase separation [6,7] and salt leaching [8], biomimetic scaffolds simulating the architectures of extracellular matrix (ECM), have lately developed as a favorable group of constructs for tissue regeneration [9]. Various techniques have been applied to develop 3D biomimetic scaffolds consisting of electrospinning [10] and rapid prototyping (RP) [11,12] methods. Recently, fabrication of scaffolds using sacrificial templates has been reported to mimic various tissues [13–15]. In this technique, the sacrificial templates act as a place holder and pore former within the precursor slurry [16]. Various types of synthetic and organic materials are applied as the sacrificial templates consisting of paraffin [17], polyurethane sponge [18] and natural 3D nanofibrous bacterial cellulose [19] for bone tissue engineering. Between them, the hard skeletons of animals and other organisms are new and inexpensive constructs which could be useful as the sacrificial templates. Between them, cuttlefish with lamellar structure of calcium carbonate (Aragonite) has recently been widely applied as a source of hydroxyapatite (HA) [20,21]. In addition to chemical composition, the homogeneous and interconnected porous structure of cuttlefish bone (90% porosity) could make it promising as a sacrificial template for fabrication of scaffold [20,22]. Moreover, in contrary to most of previous sacrificial templates, the remaining of the trace amounts of cuttlefish bone could not show diverse effects on the cell function [20,22].

Various types of ceramics (i.e. HA [23], forsterite [24], diopside [25], bredigite [23], wollastonite [26]) and polymers (i.e. chitosan [27], polycaprolactone (PCL) [8,28], poly(lactic-co-glycolic) acid

---

* Corresponding author.
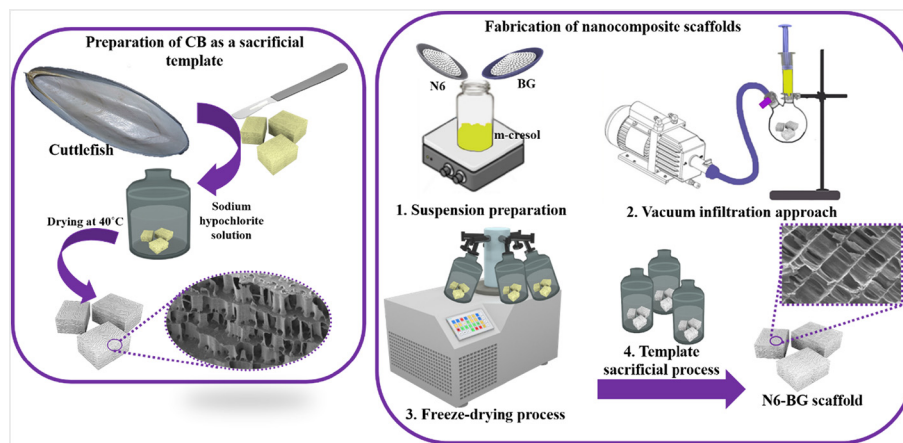  *E-mail address:* kharaziha@cc.iut.ac.ir (M. Kharaziha).

**Fig. 1.** The schematic showing the procedure of N6-BG scaffolds.

(PLGA) [29]) and their combinations have been applied for bone tissue engineering. Recently, baghdadite ($Ca_3ZrSi_2O_9$, BG), as a calcium silicate ceramic containing zirconium, has been considered as an appropriate material to build scaffolds for bone tissue engineering applications due to its excellent mechanical properties, in vitro and in vivo bioactivity, resorbability, biocompatibility and increased cell interaction compared to HA [30]. However, its brittleness and poor mechanical stability have resulted in the development of various nanocomposite materials consisting of BG as a bioactive filler in a polymer matrix [31–33]. For instance, Karamian et al. [33] developed HA-BG nanocomposite scaffolds coated by PCL/Bioglass and found that BG enhanced the mechanical strength of HA and the precipitation of bone-like apatite during the soaking in simulated body fluid.

In another word, in order to improve the biofunctionally of scaffolds for bone tissue engineering, the polymer matrices need to have desirable mechanical properties, biocompatibility and biodegradation. Nylon 6 (N6) as a synthetic polymer, has been recently used as a biomaterial in tissue engineering applications, due to its biocompatibility as well as physical and mechanical properties [34,35]. Nirmala et al. [36] developed chitosan blended N6 nanofibrous membranes. They found that while N6 fibrous membrane revealed good biocompatibility, incorporation of chitosan improved its biological properties. In another study, Shen et al. [37] reported the appropriate mechanical properties of biphasic calcium phosphate/N6. N6 structurally mimics the collagen protein in its backbone structure and reveals supreme mechanical properties due to the powerful hydrogen bonding between the chains and high regularity in the crystalline phase provide. Moreover, due to high polarity, it may create chemical bonds with inorganic fillers [38–41]. In order to control the degradation rate of this polymer, limited researches have focused on the nanocomposite scaffolds based on N6 polymers.

The aim of this research was to develop novel biomimetic nanocomposite scaffolds consisting of N6 with high mechanical properties and BG having great biological properties using a cuttlefish bone sacrificial template-based technique. Moreover, the role of various amounts of BG nanopowder on the physical, mechanical and biological properties of the scaffolds was studied. It is expected that the combination of cuttlefish bone with highly interconnected porosity could provide a promising scaffold for bone tissue engineering applications.

## 2. Material and methods

### 2.1. Synthesize of baghdadite nanopowders

Baghdadite ($Ca_3ZrSi_2O_9$, BG) nanopowder was synthesized by the sol–gel technique, as previously described [31]. Firstly, tetraethyl orthosilicate (TEOS, $(C_2H_5O)_4Si$, Sigma-Aldrich Co), ethanol (Merck) and 2 M $HNO_3$ (Sigma-Aldrich) with the molar ratio of TEOS:Ethanol:$HNO_3$ equals to 1:8:0.16 were mixed by stirring for 30 min. Afterward, zirconia oxide nitrate ($ZrO(NO_3)_2$, Sigma Aldrich Co) and calcium nitrate tetrahydrate ($Ca(NO_3)_2 \cdot 4H_2O$, Sigma Aldrich Co) were added into the mixture (molar ratio: $ZrO(NO_3)_2$:$Ca(NO_3)_2 \cdot 4H_2O$:TEOS = 1:3:2) and solution was stirred for 5 h at room temperature. Following the reaction, the obtained clear solution was kept at a constant temperature of 60 °C for 1 day and dried at 100 °C for 2 days to obtain a dry gel. Eventually, the gel was calcined at 1150 °C for 3 h to obtain the BG powder. The powder was milled using a planetary ball mill (Retsch PM 400, Germany) for 1 h with rotational speed of 250 rpm, to provide uniform particle size.

### 2.2. Preparation of the cuttlefish bone blocks as the sacrificial template

Cuttlefish bone (CB) used in this study was obtained from Persian Gulf (19 cm long). This bone contains a thick external wall and an internal lamellae matrix. The internal layer consists of parallel sheet structure which interconnected, leading to its greatly porous characteristic. Therefore, the dorsal shield was removed and the remaining lamellar segment was carefully cut into small pieces with appropriate shape and dimensions (5 mm × 5 mm × 7 mm) using a lancet. The samples were consequently treated with 8% aqueous solution of sodium hypochlorite (NaClO, Sigma-Aldrich) for 12 h at room temperature in order to remove organic components. After washing with distilled water, the CB blocks were dried at 40 °C for 48 h.

### 2.3. Fabrication of N6-BG nanocomposite scaffolds

The procedure of N6-BG scaffold fabrication is schematically presented in Fig. 1. Primarily, 10 wt% N6 (Nylon 6, Sigma-Aldrich) solution in m-cresol (Sigma-Aldrich) and various amounts of BG powder (0, 3, 5 and 10 wt%) was prepared, mixed for 5 h at 30 °C and subsequently ultra-sonicated for 4 h to get homogeneous solution. Consequently, as prepared and dried CB blocks were put in a flat-bottom flask with stopcock septum port connected to the vacuum system. Afterwards, the stopcock was opened to suck the N6-BG/m-cresol solution over the porous CB. The aim of impregnation in a vacuum was to ensure that the solutions could easily flow into the pores via removing the air out of them. After 4 h, the vacuum was stopped to allow the air pressure to force the N6-BG/m-cresol solution into the pores of the CB. In the next step, as prepared N6-BG/m-cresol/CB system was soaked in pure acetone (Sigma-Aldrich) to remove the m-cresol and then immersed them in distilled water. The N6-BG/CB complex was freeze-dried for 8 h to remove the water and the remained solvent, completely. After that, the CB was gently removed from the system by soaking the N6-BG/CB samples in 0.2 M HCl solution for 5 days. The solution was refreshed

every two days. Finally, the scaffolds were dried by heating at 35 °C for 1 day. According to BG content (0, 3, 5 and 10 wt%), the samples were named as N6-0BG, N6-3BG, N6-5BG and N6-10BG, respectively.

### 2.4. Characterization of N6-BG nanocomposite scaffolds

The morphology of BG nanopowder and scaffolds as well as the BG distribution in the scaffolds were investigated using scanning electron microscopy (SEM, Philips, XL30) equipped with energy dispersive spectroscopy (EDS). Before SEM imaging, the samples were sputter coated via a thin film gold. Furthermore, the range of pore size of scaffolds was measured from the SEM images by image analysis software (Image J, National Institutes of Health, USA). Moreover, transmission electron microscope (TEM, EM208S) was applied to evaluate the morphology and particle size of the BG powders. The phase composition of the CB, BG powder and the scaffolds was investigated using X-ray diffraction technique (XRD, X0 Pert Pro X-ray diffractometer, Phillips, Netherlands). Furthermore, the average crystallite size of the BG nanopowder was estimated by using Scherrer equation (Eq. (1)) [42]:

$$\ln \beta = \ln \frac{k\lambda}{L} + ln \frac{1}{\cos \theta} \tag{1}$$

where λ is the wavelength of Cu Kα radiation (1.5404 Å), θ is the diffraction angle (°), β is the full width of the peaks at half-maximum for the BG and L is the crystallite size (nm).

Moreover, the functional groups of CB, BG nanopowder and the scaffolds were determined by Fourier transform infrared spectroscopy (FTIR, JASCO 680 PLUSE) in the 400–4000 $cm^{-1}$ range. In addition, the porosity of the scaffolds was measured via Archimedes' method, according to the following equation (Eq. (2)) [43]:

$$\text{Porosity percentage} = \left( \frac{W_w - W_D}{W_w - W_S} \right) \times 100 \tag{2}$$

where $W_w$ is the wet weight, $W_D$ is the dry weight and $W_S$ is the wet weight of scaffolds suspended in ethanol. In order to further specify the porosity characteristics, total area fractures of porosities in different nanocomposite scaffolds were calculated from the SEM images using Image J software.

The compressive properties of the scaffolds were carried out in dry condition. The samples (n = 4) with the dimension of 5 mm × 5 mm × 7 mm were compressed to 70% of strain using a universal testing machine (Hounsfield, H25KS) with a load cell capacity of 1 kN and rate of 0.5 mm.s$^{-1}$. The stress-strain curves were plotted and then compressive modulus and compressive strength were calculated. Compressive modulus was estimated from the slope of the linear section of the stress-strain curves. Moreover, the compressive strength was determined at the maximum point of each curve. Furthermore, thermogravimetric analysis (TGA) (Rheometric scientific) was performed to determine the actual weight of the loaded BG nanopowder in the scaffolds.

### 2.5. In vitro bioactivity evolution of N6-BG nanocomposite scaffolds

In vitro bioactivity of samples was evaluated via soaking in simulated body fluid (SBF) solution, prepared as described by Bohner et al. [44]. N6-BG scaffolds consisting of various amounts of BG nanopowder (n = 4) with dimension of 5 mm × 5 mm × 10 mm were immersed in SBF solution (pH 7.4) at 37 °C for 21 days. During the soaking, the pH value of SBF solutions was measured using a pH meter (Metrohm, Switzerland 827). Moreover, SEM, EDS and XRD analysis were applied to investigate the apatite-formation ability on the surface of samples. In addition, the concentration of Ca and P ions of SBF solution was estimated after 21 days soaking of samples, using inductively coupled plasma atomic emission spectroscopy (ICP-AES) (AES; Varian, USA).

### 2.6. The degradation rate evaluation of N6-BG nanocomposite scaffold

In vitro degradation was also investigated by immersing the pre-weighed scaffolds from each N6-BG scaffold (n = 3) in phosphate buffer saline solution (pH 7.4) at 37 °C. After 3, 7, 14, 21 and 28 days, the samples were removed from the PBS solution, washed in distilled water and dried in vacuum oven at 37 °C for 24 h. The weight loss was calculated by the following equation (Eq. (3)) [45].

$$\text{Weight loss (\%)} = \frac{W_0 - W_t}{W_0} \times 100 \tag{3}$$

where $W_0$ is the initial weight of N6-BG scaffolds and $W_t$ is the dry weight after t time (3, 7, 14, 21 and 28 days) of degradation test. In addition, the surface morphology of the scaffolds after 28 days soaking in PBS solution was investigated via SEM technique, as described before.

### 2.7. Cell culture

To investigate the biocompatibility of the nanocomposite scaffolds, MG63 cell-line, purchased from Royan Institute, Iran, was applied. The cells were cultured in complete culture medium consisting of DMEM supplemented with10% fetal bovine serum (FBS) and 1% streptomycin/penicillin at 37 °C and 5% CO$_2$ in a humidified atmosphere. All components were supplied by Bioidea, Iran. Prior to cell seeding, 3D nanocomposite scaffolds were sterilized in 70% ethanol solution and ultraviolent (UV) radiation exposure. Subsequently, 5000 cells/well were seeded on the samples (n = 3) and tissue culture plate (TCP, control) and incubated at 37 °C and 5% CO$_2$ for 5 days. Culture medium was refreshed every 2 days.

To study the morphology of the cells seeded on the samples, after 5 days of culture, the scaffolds were washed with PBS solution and were fixed using 2.5% glutaraldehyde (Sigma). Consequently, the samples were dehydrated in various concentrations of ethanol solution (30, 50, 70, 90 and 96%) for 10 min, respectively. Finally, the samples were dried in a desiccator overnight and the morphology of cells was examined using SEM imaging. The relative viability of cells cultured on the 3D scaffolds was investigated using 3-(4,5-dimethylthiazol-2-yl)-2,5-diphenyltetrazoliumbromide (MTT) assay (Sigma). After 1, 3 and 5 days, the culture medium was discarded and MTT solution (0.5 g/ml) was added to the samples (n = 3) and control. After 4 h incubation, as-prepared dark blue formazan crystals were dissolved in dimethyl sulfoxide (DMSO, Sigma) and kept for 30 min at 37 °C. Afterward, a certain amount of dissolved formazan solution of various samples was moved to a 96-well plate and the optical density (OD) of each well was measured via a microplate reader (BioTek, Model ELX800, USA) at a wavelength of 630 nm. Finally, the relative cell survival (% control) was calculated based on the Eq. (4) [46]:

$$\text{Relative cell survival (\%control)} = \frac{X_{Sample} - X_b}{X_C - X_b} \times 100 \tag{4}$$

where $X_{sample}$ is the absorbance of the samples, $X_b$ and $X_c$ are the absorbance of the blank (DMSO) and control (TCP), respectively.

### 2.8. Statistical analysis

The data in this study was evaluated via one-way ANOVA analysis using GraphPad Prism Software (V.6) and were expressed as mean ± standard deviation (SD) in each experiment. Differences were determined statistically significant with a P-value < 0.05.

## 3. Result and discussion

### 3.1. Characterization of baghdadite nanopowder

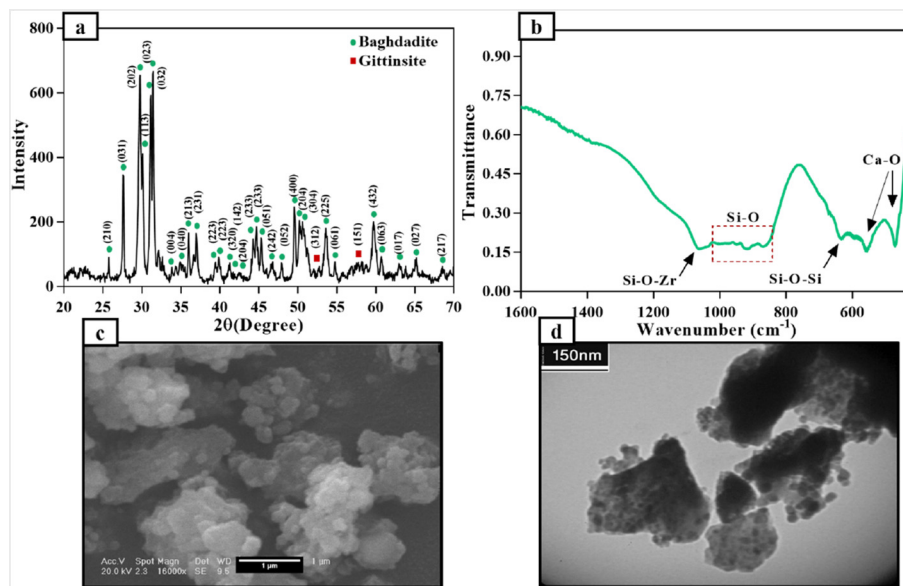Before fabrication of nanocomposite scaffolds, BG nanopowder was

**Fig. 2.** Characterization of BG nanopowder synthesized via sol-gel process: (a) XRD pattern, (b) FTIR spectrum, (c) SEM image and (d) TEM micrograph of BG nanopowder.

synthesized. XRD pattern of BG nanopowder (Fig. 2a) shows that there is a good agreement with the standard card of pure BG (JCPD: 00-047-1854) and the synthesized powder, conforming BG nanopowder was synthesized as the main phase. However, the secondary phase with insignificant intensity could also be detected which was related to Gittinsite (JCPD: 01-084-2099). Furthermore, the average crystallite size of the BG nanopowder calculated by Scherrer equation was estimated about $24 \pm 1$ nm. FTIR spectrum of nanopowder (Fig. 2b) also confirmed the formation of BG nanopowder. The spectrum consisted of two characteristics peaks at 450–600 $cm^{-1}$, attributed to Ca−O bond and the absorption peak centering at 636 $cm^{-1}$, related to the vibration of the Si−O−Si group. In addition, the peaks covering the range of 800–1250 $cm^{-1}$ revealed the presence of the isolated groups of $SiO_4$. Furthermore, the peaks detected in the frequency of 1050 $cm^{-1}$ were corresponded to the Si−O−Zr vibration [47,48]. SEM image (Fig. 2c) also showed BG nanopowder had a spherical morphology with the agglomerated particles smaller than $0.83 \pm 0.03$ µm. In addition, according to TEM image (Fig. 2d), BG nanopowder consisted of spherical-like particles in the range of 19–29 nm. The average size of BG nanoparticles was also estimated about $23 \pm 3$ nm.

### 3.2. Characterization of cuttlefish bone

Cuttlefish bone was applied as the sacrificial template for the fabrication of the scaffolds. Fig. 3a, b shows the structure of row internal cuttlefish bone in perpendicular direction to the lamellas in different magnifications confirming the presence of thin organic component (β-chitin) between the inorganic materials (aragonite) in the main structure (indicated by red arrow) [20]. This organic component was removed after soaking the CB structure in NaClO overnight (Fig. 3c and d). As a consequence, the lamella structure of CB consisting of numerous regular parallel sheets separated by pillars was discovered, which was similar to previous studies [20]. This natural porous structure with interconnected porosities (Fig. 3d) comprised of pores with size of $274 \pm 68$ µm in the long axis and $83 \pm 13$ µm in the minor axis of the pores. Moreover, the porosity of CB was estimated about $91 \pm 2\%$. This structure could be beneficial to facilitate the nutrients transfer, cell ingrowth and migration [49].

XRD patterns of CB structure, before and after NaClO treatment, are also presented in Fig. 3e. XRD pattern of untreated CB consisted of the aragonite phase (JCPD: 96-901-3802). However, compared to the

standard aragonite phase, the relative intensity of the peaks extraordinarily changed which could be due to the particular layered structure of aragonite established via the biomineralization of CB in the sea [21]. Moreover, XRD patterns also confirmed the absence of the extra phases relevant to calcite or other oxide phases. After NaClO treatment, XRD pattern of CB was not changed confirming that organic removing did not impress the chemical structure of CB. FTIR spectrum of CB (Fig. 3f) also confirmed the aragonite structure of CB. A doublet peaks at 700 and 712 $cm^{-1}$ were related to the in-plane bending mode of C−O ($\nu_4$ mode) of aragonite. Moreover, the characteristic peaks at 857 $cm^{-1}$ and 1082 $cm^{-1}$ could be related to the C−O out-of-plane bending ($\nu_2$ mode) and carbonate symmetrical plane bending ($\nu_1$ mode) vibration, respectively. Finally, the strongest peak centered at 1490 $cm^{-1}$ was corresponded to asymmetrical stretching ($\nu_3$ mode) of aragonite structure [50].

### 3.3. Characterization of N6-BG nanocomposite scaffolds

SEM images of various N6-BG scaffolds containing 0 wt% BG (N6-0BG), 3 wt% BG (N6-3BG), 5 wt% BG (N6-5BG) and 10 wt% BG (N6-10BG), after CB removal are presented in Fig. 4a. It was found that pure polymeric and all nanocomposite scaffolds consisted of elliptical macropores similar to CB structure. Particularly, the scaffold consisting of 10 wt% BG could mimic the chamber-like microstructure of CB with high length-to-width ratio. Furthermore, higher magnification images of nanocomposite scaffolds confirmed the formation of interconnected pores.

The role of BG concentration on the porosity of the scaffolds was also evaluated via Image J software (Fig. 4b, c). Results showed that the porosity of the scaffolds (Fig. 4b) significantly decreased from $90 \pm 2\%$ to $70 \pm 1\%$ and area fraction of porosities (Fig. 4c) reduced from $76 \pm 2\%$ to $57 \pm 4\%$, as the BG content increased from 0 to 10 wt% ($P < 0.05$), partly owing to more BG content that coat on the skeleton of the N6 matrix and thus hamper the pore growth [51]. It should be noted that this porosity is high enough to be applied in the field of bone tissue engineering scaffold [52]. Diba et al. [53] fabricated the forsterite-PCL nanocomposite scaffolds via solvent-casting/particle-leaching method, and found that the porosity of scaffolds reduced with increasing forsterite content. Moreover, the range of pore size in long axis (Supplementary Fig. S1) was not significantly changed. For instance, pore size in long axis of N6-0BG was 130–240 µm which was
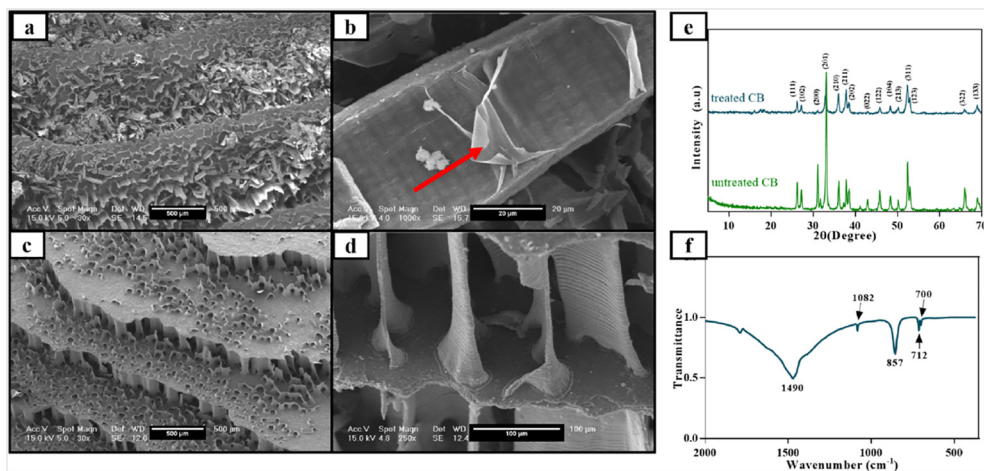
**Fig. 3.** Characterization of CB, before and after treatment: SEM images of (a, b) row internal CB and (c, d) treated CB using NaClO, in the perpendicular direction to the lamellas. (e) XRD patterns of CB before and after treatment with NaClO, (f) FTIR spectrum of treated CB. (For interpretation of the references to color in this figure, the reader is referred to the web version of this article.)

changed to 180–340 μm (N6-3BG), 180–225 μm (N6-5BG) and 153–253 μm (N6-10BG), after incorporation of BG nanopowder. This pore size distribution shifted to lower values as the BG content increased in the nanocomposite scaffolds, indicating that the addition of BG assisted in the formation of pores with smaller sizes in both long and minor axis. The importance of this effect was examined via assessment of the average pore size of the scaffolds in the long and minor axis (Fig. 4d). It could be found that while all scaffolds revealed a slightly larger pore size in the long axis than in the minor axis, due to morphology of CB template, N6-BG scaffolds revealed lower pore sizes in both the long axis and the minor axis and this difference enhanced with increasing BG content. These results further confirmed the significant effect of BG on the formation of a chamber-like pore structure mimicking the CB structure. Zhou et al. [54] fabricated HA/Ethylene-Vinyl Acetate/Polyamide 66 composite scaffolds by the injection-molding method. The results showed that the pore size of the scaffolds decreased with increasing HA content. According to above results, we could conclude that the microstructure of N6-BG scaffold consisting 10 wt% BG was favorable, owing to highly porous structure with a well-developed network of interconnected pores. According to previous results, the highly porous structure could stimulate the osteogenesis in vivo, as bone regeneration comprises penetration of cells from the surrounding tissue and vascularization. Moreover, 100 μm is typically selected as the minimum prerequisite for pore size to allow cell migration, vascularization, and transport procedures [55].

Fig. 5a shows the amounts of Ca, and Zr elements in the N6-BG scaffolds consisting of 3, 5 and 10 wt% BG, extracted from EDS analysis. Results showed that BG nanopowder containing Ca and Zr was well

distributed in the N6 matrix, Moreover, atomic percentage of Ca increased from 10% to 36% and atomic percentage of Zr enhanced from 3% to 10% as the amount of BG in the scaffolds increased from 3 to 10 wt%, respectively (Fig. 5b). It could be found that the Ca/Zr ratio was near to that of BG confirming the presence of this component in the structure. However, Ca/Zr ratio enhanced to about 3.6 at N6-10BG scaffold which might be due to the presence of residual mass of CB template. The reduced pore size of N6-10BG (Fig. 4) might prevent from the complete removing of the CB from the scaffold.

To confirm the incorporation of BG nanopowder in the N6 scaffold, XRD patterns of various scaffolds consisting of different amounts of BG were investigated (Fig. 6a). Two sharp peaks appeared at 2θ = 20.2° (200 reflection) and 23.6° (002 and 202 reflection) were corresponded to the α-phase of pure N6 polymer, confirming that the final treatment for removing the CB scaffold did not change the N6 polymer property. There were no peaks corresponding to another crystalline phase such as γ and β-crystallite phase in pure N6 and polymer scaffolds [56]. Two characteristic peaks of BG nanoparticles appeared at 2θ = 28.3° and 31.5° in N6-10BG scaffold, confirming the presence of BG nanoparticles in the scaffold. Moreover, N6 revealed two strong peaks at 2θ = 20.2° (200) and 23.6° (002, 202 doublet) related to the α-crystalline form of N6. Our results indicated that the intensity of two characteristic peaks of N6 decreased significantly, with increasing BG content. It might be due to the interaction occurred between N6 and BG nanoparticles leading to disarrangement of the hydrogen bonded sheets of the α-phase related to N6 leading to reduced crystallinity of N6 [57].

FTIR spectrum of pure N6 and BG powders as well as N6-0BG and N6-10BG scaffolds in the range of 400–4000 cm$^{-1}$ presented in Fig. 6b
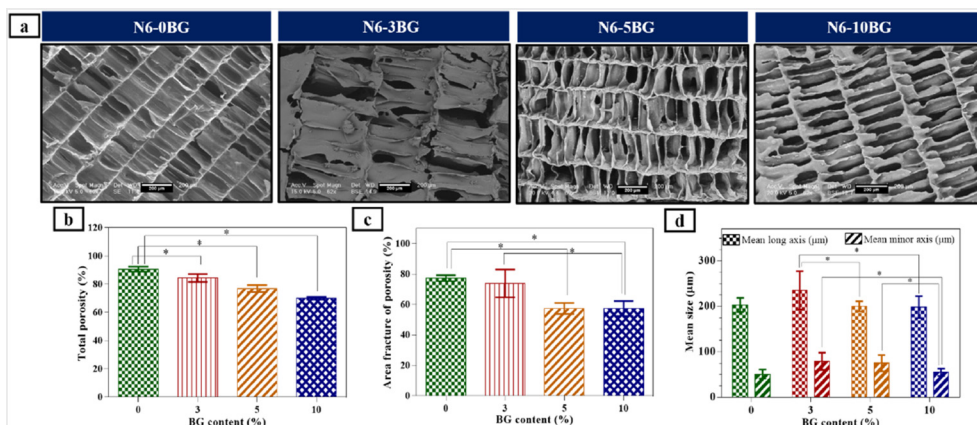


**Fig. 4.** (a) SEM images of N6-BG scaffolds containing various amounts of BG (0, 3, 5 and 10 wt%). Values of (b) the total porosity and (c) the area fracture of pores of N6-BG scaffolds. (d) Mean long axis pore size and minor axis pore size of N6-BG scaffolds with different amounts of BG.
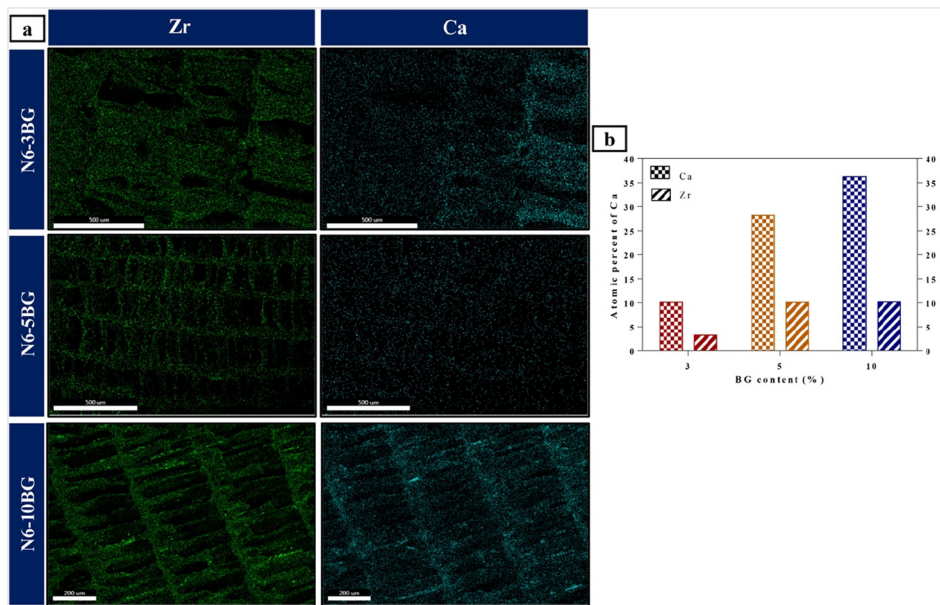
**Fig. 5.** (a) EDS mapping and (b) values of atomic percentage of Ca and Zr of nanocomposite scaffolds consisting of different BG contents, after CB removal.

also revealed the characteristic peaks of N6 at 3270 cm$^{-1}$ attributed to N−H stretching vibration, at 1670 cm$^{-1}$ and 1552 cm$^{-1}$ related to C═O stretching vibration (amide *I* band) and the combination of N−H bending vibration and C−N stretching vibration (amide *II* band), respectively [58]. Moreover, a pair of peaks at ~2920 and 2852 cm$^{-1}$ were related to C−H bond [59]. It could be concluded that some adsorption peaks of N6 changed in the scaffolds. For instance, amide II bond recognized at about 1535 cm$^{-1}$ slightly moved to lower wavenumber after incorporation of BG nanopowder, confirming molecule interaction such as hydrogen bonding formed between the BG and N6 [58]. Furthermore, the absorption bands detected at 690 cm$^{-1}$ and 850 cm$^{-1}$ were attributed to Si−O−Si and Si−O vibrations of BG, respectively, confirming the presence of BG in the composite scaffold. Moreover, a new peak could be detected at 1380 cm$^{-1}$ corresponded to −COO$^{-}$ stretching vibration in the nanocomposite. It might be due to the interaction between Ca of BG and the −COO group of N6. These interactions could have robust effect on the interface performance and mechanical characteristics of the nanocomposite [60]. In addition, compared to the spectra of N6 and BG powders, the characteristic peaks

of the components were not significantly modulated, confirming inability of the treatment processes to deteriorate these structures.

In order to estimate the actual amounts of BG in the scaffolds (N6-0BG, N6-5BG and N6-10BG), TGA was performed and the remained weight of scaffolds after completely burning out of N6 content was estimated (Fig. 6c). It could be found that all scaffolds were stable up to 390 °C and consequently decomposed. The decomposition temperature range of all scaffolds was in the range of 397–507 °C. In addition, the TGA thermograms revealed that all scaffolds revealed different residual content, depending on the BG content. While N6-0BG scaffold left < 2% residual content, it was significantly enhanced to 5.8% and 10.2% for N6-5BG and N6-10BG, respectively. Our results demonstrated that the BG nanopowder theoretically added to the polymer solution was approximately near to that of in the scaffolds.

### 3.4. Mechanical behavior of N6-BG scaffolds

The synthetic scaffolds for tissue engineering applications must have mechanical properties as close as possible to that of surrounding
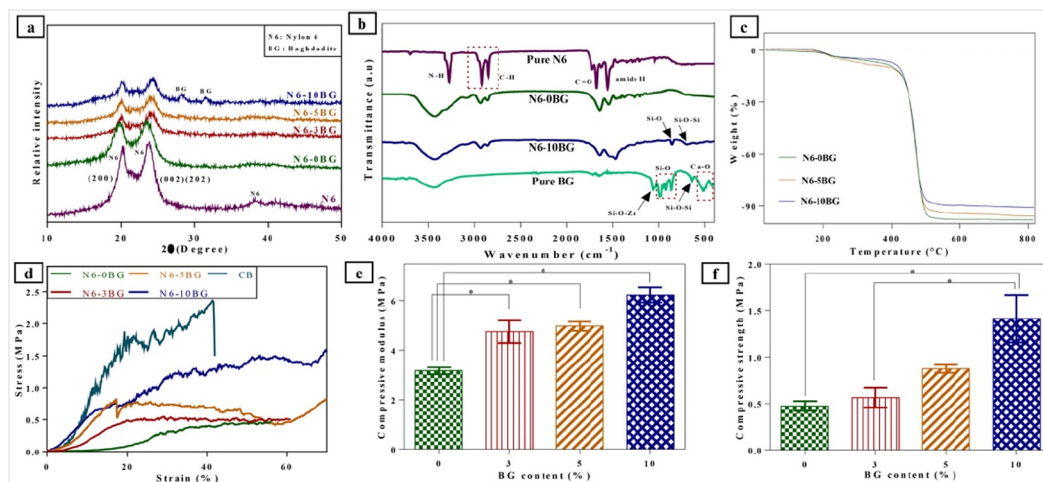


**Fig. 6.** Characterization of N6-BG Scaffolds: (a) XRD patterns of pure N6 and N6-BG scaffolds consisting of various amounts of BG, (b) FTIR spectra of pure N6 and BG powders as well as N6-0BG and N6-10BG scaffolds. (c) TGA analysis of nanocomposite scaffolds consisting of 0, 5 and 10 wt% BG. (d) Stress-strain curve, (e) compressive strength and (f) compressive modulus of nanocomposite scaffolds (*: *P* < 0.05).

tissue. Fig. 6d represents the stress-strain curves of N6-BG nano-composite scaffolds containing 0, 3, 5 and 10 wt% BG. The stress-strain curve of CB structure was also presented compared with scaffolds. Our results showed that the CB structure revealed a typical brittle behavior. The stress-strain curve related to CB consisted of an initial linear portion, a maximum stress point and catastrophic failure occurred. All stress-strain curves related to 3D scaffolds were almost identical, showing the stages of initial stiff deformation at small strain followed by yield point and a nearly constant stress plateau at significantly large strain. The third portion of the curves was only well-defined for the scaffolds containing 5 and 10 wt% BG (N6-5BG, N6-10BG). During the compression stress, the cells started to collapse at an approximately invariant load by elastic buckling, or fracture, depending on the cell wall component. When all cells collapsed, additional deformation presses differing cell walls against each other leading to increase the stress severely. This last stage is referred to as densification [61]. According to the stress-strain curves, compressive strength (Fig. 6e) and compressive modulus (Fig. 6f) were estimated. Our results revealed that the compressive strength and compressive modulus significantly enhanced from $0.47 \pm 0.05$ MPa to $1.41 \pm 0.25$ MPa and from $3.16 \pm 0.14$ MPa to $6.23 \pm 0.3$ MPa, respectively, with increasing BG content upon 10 wt% ($P < 0.05$). The compressive strength of nano-composite scaffolds specially N6-10BG was in the range of compressive strength of cancellous bone. It is clear that the presence of BG nano-powder as a stiff filler improved the mechanical behavior of composite scaffold. The improved mechanical properties of the nanocomposite scaffolds could be due to the uniform distribution of BG in the N6 matrix without any agglomeration and interface interaction between N6 and inorganic BG phase. In addition, reduced porosity of nano-composite scaffolds with increasing BG content could result in improved mechanical properties of the scaffolds. This result was similarly reported in previous studies. For instance, Shen et al. [37] found that the addition of biphasic calcium phosphates (BCP) as a hard re-inforcement in the N6 scaffold increased the compressive strength from 0.62 MPa to 1.86 MPa. However, the relatively low compressive modulus reported for the scaffolds in this report could be attributed to the special pore structure and high porosity acquired with the scaffold fabrication procedure. Moreover, it could be found that both compressive strength and compressive modulus were less than those of CB structure reported before, conforming the CB removal from the scaffolds.

### 3.5. In vitro bioactivity and biodegradation evaluation of N6-BGs scaffolds

In order to investigate the ability of the scaffolds to in vivo bone formation stimulation, in vitro bioactivity was performed [62]. The apatite formation ability of N6-BG scaffolds was investigated via soaking in SBF solution for 21 days at $37 \pm 0.5$ °C. The surface morphology and EDS spectrum of the samples after 21 days soaking are shown in Fig. 7a and b. Results revealed the precipitation of calcium phosphate nodules on the scaffold surfaces after immersion in SBF for 21 days. However, the morphology of these precipitates was different, depending on the BG content. While the surface of N6-0BG scaffold was completely covered by ball-like particles, needle like precipitates along with cauliflower-like particles were covered N6-BG scaffolds. These morphologies were similarly detected for other nanocomposite bioactive scaffolds [62]. The EDX spectrum of these samples confirmed that shows these particles were composed of calcium and phosphorus with various atomic percentages, depending on the BG content in the scaffolds. It needs to mention that because of overlapping of gold and phosphorus peaks, the exact amounts of phosphorus could not be measured, correctly. Nevertheless, the EDS spectra indicated that calcium atomic percentage increased as a function of BG content. For example, Ca atomic percentage of N6-3BG and N6-10BG scaffolds was 1.8% and 3.4%, respectively. Moreover, XRD pattern of N6-10BG scaffold after 21 days of soaking in SBF solution (Fig. 8a) confirmed the

presence of HA on the scaffold surface after 21 days of soaking in SBF solution.

The variations of pH value of SBF solution during 21 days soaking of the scaffolds are illustrated in Fig. 8b. While the pH value of SBF solution during soaking of N6-0BG scaffold was not significantly changed, it slightly enhanced during the soaking of nanocomposite scaffolds, and consequently reduced and reached a stable value. The profile changes of pH in SBF solution was similar to that of the CaO–SiO$_2$ based bioactive ceramics (such as wollastonite [63] and diopside [64]). Hence, the apatite formation mechanism on the 3D scaffolds containing BG might be similar to that of CaO–SiO$_2$ based bioactive ceramics. The increase in the pH value in the first 10 days might be due to the release of $Ca^{2+}$, $Zr^{4+}$ and $Si^{4+}$ ions in SBF solution, exchange of these ions with $H^+$ or $H_3O^+$ of the solution and formation of negatively charged groups of silanol (Si−OH) and Zr−OH [48]. Consequently, nucleation of Ca−P was performed leading to the formation of bone-like apatite on the surface of scaffolds. In order to investigate the changes of Ca and P concentration in SBF solution, after 21 days of soaking of samples, ICP test was performed. According to Fig. 8c, due to the migration of Ca and P elements during the deposition of bioactive minerals on the surface, the concentration of the mentioned elements decreased compared to control group (the concentration of Ca and P in SBF solution was 2.5 mM and 1 mM, respectively). Furthermore, the concentration of phosphorous and calcium ions reduced as a function of BG content in various scaffolds confirming the enhanced bioactivity of samples. For instance, while the concentration of phosphorous and calcium ions of the solution containing N6-0BG sample was about 0.54 and 1.3 mM, respectively, they were reduced to 0.43 and 0.86 mM, respectively, when N6-10BG sample was soaked.

In vitro degradation behavior of scaffolds is a significant factor in bone tissue regeneration. Fig. 8d shows the weight loss of the N6-BG scaffolds consisting of various amounts of BG in PBS solution as a function of immersion time. Our result revealed that pure polymeric scaffold did not show any significant weight loss. The weight loss of N6-0BG scaffold after 28 days of soaking in PBS was only about $4.5 \pm 1$ wt %. The previous studies also revealed that N6 was mainly non-de-gradable, due to its powerful inter-chain interactions caused by the hydrogen bonds between molecular chains and high regularity in the crystalline phase [41]. In contrary to pure polymeric scaffold, the weight loss of N6-BG scaffolds enhanced as a function of soaking time and BG content. Noticeably, after 28 days of soaking, the weight loss of N6-10BG scaffold reached to $15.4 \pm 2$ wt%. The enhanced weight loss of nanocomposite scaffolds with increasing BG content might be due to hydrophilic nature of BG nanopowder. Consequently, enhanced PBS absorption resulted in greater ion release leading to enhanced amide bond breakage due to higher amorphous regions and hydrolysis of polymeric parts of nanocomposites.

### 3.6. Cell culture

To determine the role of BG nanopowder on the biological properties of N6-BG scaffolds, MG63 cells were cultured on the samples. SEM images of cells cultured on samples for 5 days are represented in Fig. 9a. The red arrows in the figures indicated the cells attached and spread on the surface of the scaffolds. Nevertheless, the cell spreading was different based on the BG concentration. The MG63 cells adhered to the surface of the nanocomposite scaffolds specially at N6-5BG and N6-10BG, while a fewer number of cells were attached on the surface of pure polymeric scaffold (N6-0BG). Moreover, most of the cells attached on the N6-0BG scaffold were spherical and agglomerated together. Previous studies revealed that the N6 polymer had no negative effect on the adherence and growth of cells due to its chemical structure mimicking that of collagen protein in extracellular matrix. In this regard, the presence of amide and carboxyl in the structure of N6 could direct the cell growth, and encourage the bone formation [65]. Our results revealed that incorporation of BG improved the cell spreading.
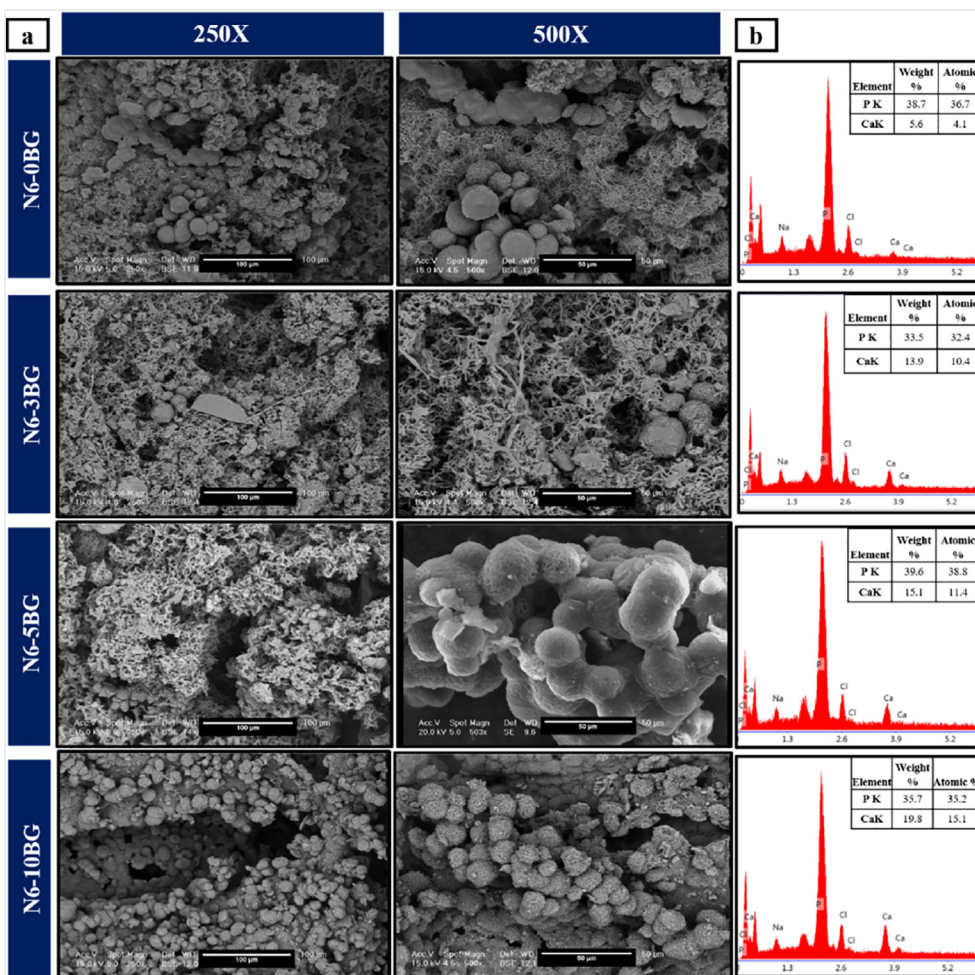
**Fig. 7.** In vitro bioactivity evaluation of N6-BG Scaffolds: a) SEM micrographs and b) EDS spectra of N6-BG scaffolds containing various amounts of BG nanopowder, after soaking in SBF for 21 days.
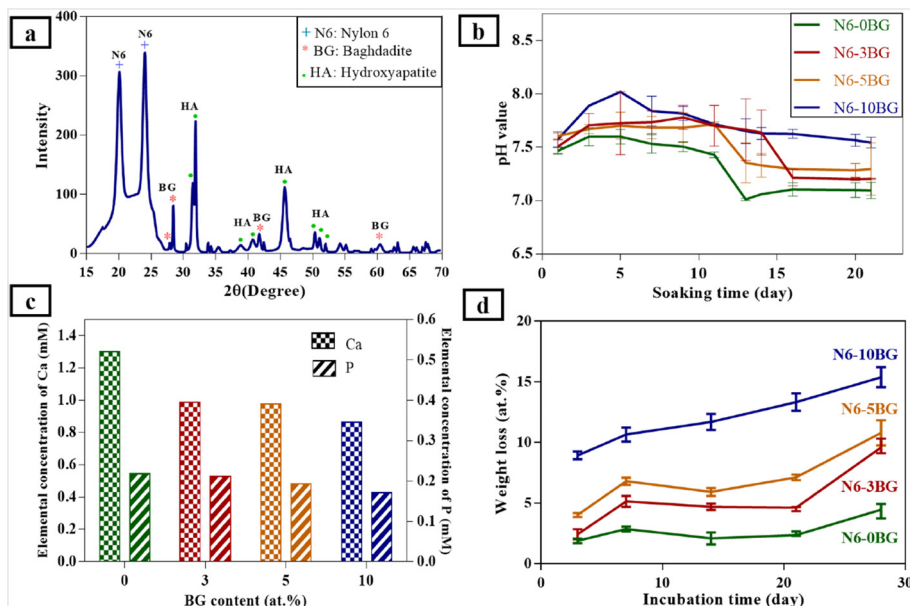


**Fig. 8.** In vitro bioactivity evaluation of scaffolds: (a) XRD pattern of N6-10BG scaffold after 21 day soaking in SBF solution. (b) pH value of SBF solution during the immersion of samples and (c) the concentration of Ca and P ions of SBF solution as a function of BG content. (d) Weight loss of the N6-BG scaffolds as a function of degradation time.
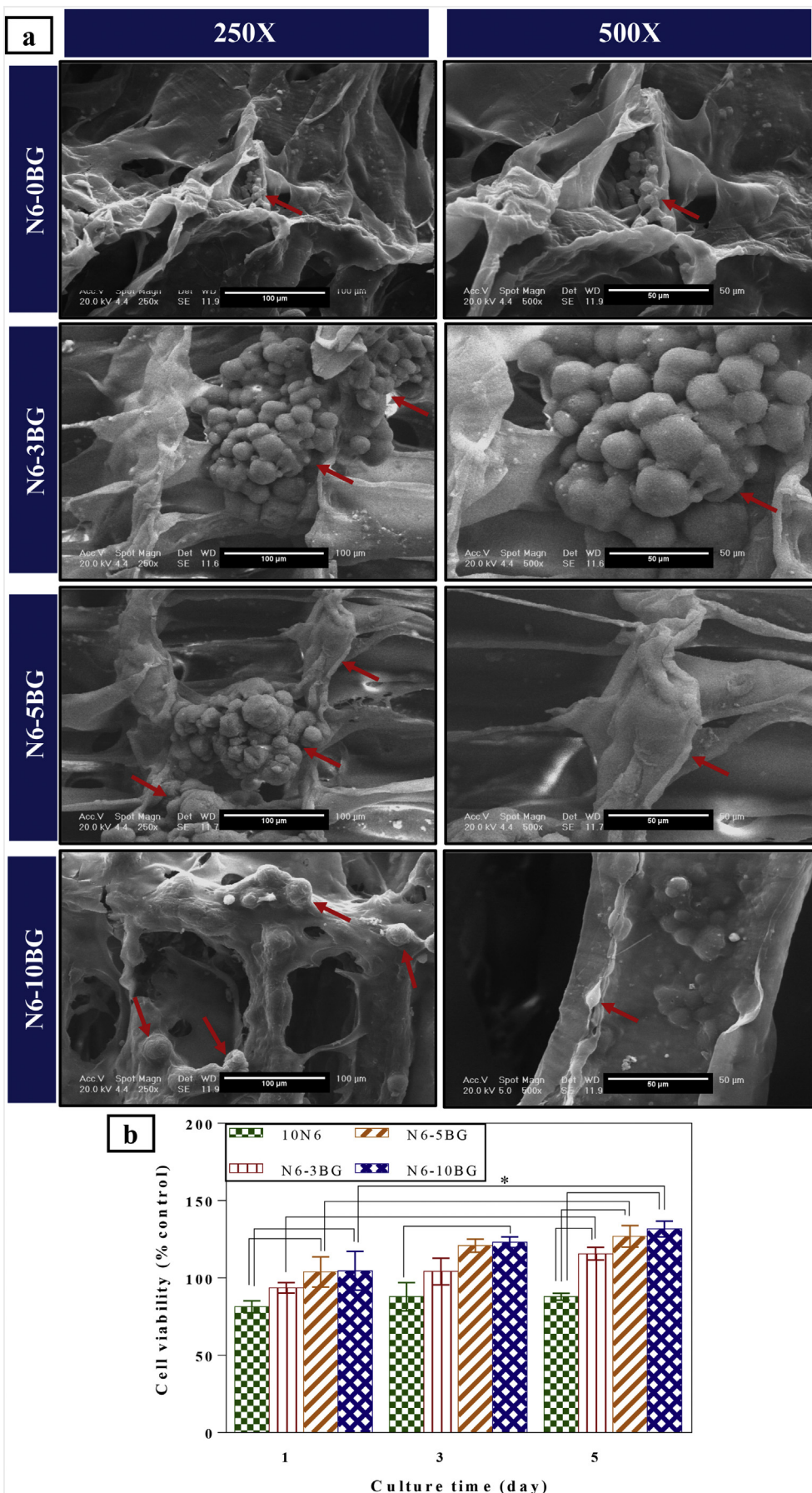
**Fig. 9.** (a) SEM images of MG63 cells after 5 days of culture. (b) The viability of cells cultured on the N6-PG scaffolds determined using MTT assay. The absorbance was normalized against control (TCP) (*: $P < 0.05$). (For interpretation of the references to color in this figure, the reader is referred to the web version of this

Moreover, the MTT assay results (Fig. 9b) revealed that the viability of cells cultured on the N6-BG increased meaningfully with increasing BG content. Moreover, it was evident that the cell viability on all scaffolds increased gradually with increasing culture time. For instance, the viability of cells cultured on the N6-10BG remarkably increased from $104 \pm 12$ (%control) to $131 \pm 7$ (%control), after 5 days of culture ($P < 0.05$). This result was similarly reported in the previous investigations on the bone cement of PMMA containing BG nanopowder [66]. This cellular behavior could be due to an increase in the concentration of Si, Ca, and Zr ions in the culture media due to the dissolution which increased the cellular activity. Recent studies revealed that the silica groups in the bioceramics provid negatively charges due to its lower isoelectric point. As a consequence, these silanol groups could interact with various functional groups facilitating the cell growth and spreading [8].

## 4. Conclusion

The aim of this investigation was to fabricate novel nanocomposite scaffolds containing N6 and baghdadite (BG) nanopowder using cuttlefish bone as the sacrificial template. The effects of N6 and BG nanopowder concentration on the physical, mechanical and biological properties of the scaffolds were studied. Incorporation of BG nanopowders to the N6 matrix resulted in the formation of the scaffolds with interconnected open pores which mimicked the chamber-like structure of cuttlefish bone. Furthermore, the incorporation of BG nanopowder to the N6 matrix improved the compressive strength and modulus of nanocomposite scaffolds comparing to pure N6 scaffolds. Moreover, BG nanopowder remarkably improved bioactivity, and degradation ability of 3D nanocomposite scaffolds. Finally, MG63 cells attachment, spreading and proliferation significantly promoted on N6-BG scaffold. Our results represented that N6-BG nanocomposite scaffolds could be an appropriate structure for bone tissue engineering at the optimal concentration of BG (10%).

Supplementary data to this article can be found online at https://doi.org/10.1016/j.msec.2019.110549.

## CRediT authorship contribution statement

**V. Abbasian:** Investigation, Writing - original draft, Visualization, Formal analysis, Software. **R. Emadi:** Supervision, Project administration, Funding acquisition, Conceptualization. **M. Kharaziha:** Project administration, Methodology, Visualization, Conceptualization.

## Declaration of competing interest

The authors certify that they have no conflict of interest to declare.

## Acknowledgements

## References

[1] S. Li, A. Abdel-Wahab, V.V. Silberschmidt, Analysis of fracture processes in cortical bone tissue, Eng. Fract. Mech. 110 (2013) 448–458.

[2] F. Loi, L.A. Córdova, J. Pajarinen, T.-h. Lin, Z. Yao, S.B. Goodman, Inflammation, fracture and bone repair, Bone 86 (2016) 119–130.

[3] C. Gao, D. Wei, H. Yang, T. Chen, L. Yang, Nanotechnology for treating osteoporotic vertebral fractures, Int. J. Nanomedicine 10 (2015) 5139.

[4] A.J. Salgado, O.P. Coutinho, R.L. Reis, Bone tissue engineering: state of the art and future trends, Macromol. Biosci. 4 (8) (2004) 743–765.

[5] Q.L. Loh, C. Choong, Three-dimensional scaffolds for tissue engineering applications: role of porosity and pore size, Tissue Eng. B Rev. 19 (6) (2013) 485–502.

[6] N. Abzan, M. Kharaziha, S. Labbaf, N. Saeidi, Modulation of the mechanical, physical and chemical properties of polyvinylidene fluoride scaffold via non-solvent

[7] N. Golafshan, H. Gharibi, M. Kharaziha, M. Fathi, A facile one-step strategy for development of a double network fibrous scaffold for nerve tissue engineering, Biofabrication 9 (2) (2017) 025008.

[8] M. Diba, M. Kharaziha, M. Fathi, M. Gholipourmalekabadi, A. Samadikuchaksaraei, Preparation and characterization of polycaprolactone/forsterite nanocomposite porous scaffolds designed for bone tissue regeneration, Compos. Sci. Technol. 72 (6) (2012) 716–723.

[9] T.G. Kim, H. Shin, D.W. Lim, Biomimetic scaffolds for tissue engineering, Adv. Funct. Mater. 22 (12) (2012) 2446–2468.

[10] M. Kharaziha, M. Fathi, H. Edris, Development of novel aligned nanofibrous composite membranes for guided bone regeneration, J. Mech. Behav. Biomed. Mater. 24 (2013) 9–20.

[11] S. Naghieh, E. Foroozmehr, M. Badrossamay, M. Kharaziha, Combinational processing of 3D printing and electrospinning of hierarchical poly (lactic acid)/gelatin-forsterite scaffolds as a biocomposite: mechanical and biological assessment, Mater. Des. 133 (2017) 128–135.

[12] M. Kharaziha, M. Nikkhah, Spatial Patterning of Stem Cells to Engineer Microvascular Networks, Microscale Technologies for Cell Engineering, Springer, 2016, pp. 143–166.

[13] J.G. Hardy, C.E. Ghezzi, R.J. Saballos, D.L. Kaplan, C.E. Schmidt, Supracolloidal assemblies as sacrificial templates for porous silk-based biomaterials, Int. J. Mol. Sci. 16 (9) (2015) 20511–20522.

[14] Q.Z. Chen, I.D. Thompson, A.R. Boccaccini, 45S5 Bioglass®-derived glass–ceramic scaffolds for bone tissue engineering, Biomaterials 27 (11) (2006) 2414–2425.

[15] J.B. Scott, M. Afshari, R. Kotek, J.M. Saul, The promotion of axon extension in vitro using polymer-templated fibrin scaffolds, Biomaterials 32 (21) (2011) 4830–4839.

[16] E. Hammel, O.-R. Ighodaro, O. Okoli, Processing and properties of advanced porous ceramics: an application based review, Ceram. Int. 40 (10) (2014) 15351–15370.

[17] Y. Liu, J.H. Kim, D. Young, S. Kim, S.K. Nishimoto, Y. Yang, Novel template-casting technique for fabricating β-tricalcium phosphate scaffolds with high interconnectivity and mechanical strength and in vitro cell responses, J. Biomed. Mater. Res. A 92 (3) (2010) 997–1006.

[18] J.M. Oliveira, S.S. Silva, P.B. Malafaya, M.T. Rodrigues, N. Kotobuki, M. Hirose, M.E. Gomes, J.F. Mano, H. Ohgushi, R.L. Reis, Macroporous hydroxyapatite scaffolds for bone tissue engineering applications: physicochemical characterization and assessment of rat bone marrow stromal cell viability, J. Biomed. Mater. Res. A 91 (1) (2009) 175–186.

[19] H. Luo, Y. Zhang, G. Li, J. Tu, Z. Yang, G. Xiong, Z. Wang, Y. Huang, Y. Wan, Sacrificial template method for the synthesis of three-dimensional nanofibrous 58S bioglass scaffold and its in vitro bioactivity and cell responses, J. Biomater. Appl. 32 (2) (2017) 265–275.

[20] J. Cadman, S. Zhou, Y. Chen, Q. Li, Cuttlebone: characterisation, application and development of biomimetic materials, J. Bionic Eng. 9 (3) (2012) 367–376.

[21] J. Rocha, A. Lemos, S. Agathopoulos, P. Valério, S. Kannan, F. Oktar, J. Ferreira, Scaffolds for bone restoration from cuttlefish, Bone 37 (6) (2005) 850–857.

[22] J. Cadman, S. Zhou, Y. Chen, W. Li, R. Appleyard, Q. Li, Characterization of cuttlebone for a biomimetic design of cellular structures, Acta Mech. Sinica 26 (1) (2010) 27–35.

[23] M. Eilbagi, R. Emadi, K. Raeissi, M. Kharaziha, A. Valiani, Mechanical and cytotoxicity evaluation of nanostructured hydroxyapatite-bredigite scaffolds for bone regeneration, Mater. Sci. Eng. C 68 (2016) 603–612.

[24] A. Forghani, M. Mapar, M. Kharaziha, M.H. Fathi, M. Fesharaki, Novel fluorapatite-forsterite nanocomposite powder for oral bone defects, Int. J. Appl. Ceram. Technol. 10 (2013) E282–E289.

[25] Y. Hosseini, R. Emadi, M. Kharaziha, Surface modification of PCL-diopside fibrous membrane via gelatin immobilization for bone tissue engineering, Mater. Chem. Phys. 194 (2017) 356–366.

[26] S. Saravanan, N. Selvamurugan, Bioactive mesoporous wollastonite particles for bone tissue engineering, J. Tissue Eng. 7 (2016) 2041731416680319.

[27] W. Thein-Han, R. Misra, Biomimetic chitosan–nanohydroxyapatite composite scaffolds for bone tissue engineering, Acta Biomater. 5 (4) (2009) 1182–1197.

[28] J.M. Williams, A. Adewunmi, R.M. Schek, C.L. Flanagan, P.H. Krebsbach, S.E. Feinberg, S.J. Hollister, S. Das, Bone tissue engineering using polycaprolactone scaffolds fabricated via selective laser sintering, Biomaterials 26 (23) (2005) 4817–4827.

[29] P. Gentile, V. Chiono, I. Carmagnola, P. Hatton, An overview of poly (lactic-co-glycolic) acid (PLGA)-based biomaterials for bone tissue engineering, Int. J. Mol. Sci. 15 (3) (2014) 3640–3659.

[30] T.C. Schumacher, E. Volkmann, R. Yilmaz, A. Wolf, L. Treccani, K. Rezwan, Mechanical evaluation of calcium-zirconium-silicate (baghdadite) obtained by a direct solid-state synthesis route, J. Mech. Behav. Biomed. Mater. 34 (2014) 294–301.

[31] S. Roohani-Esfahani, C. Dunstan, B. Davies, S. Pearce, R. Williams, H. Zreiqat, Repairing a critical-sized bone defect with highly porous modified and unmodified baghdadite scaffolds, Acta Biomater. 8 (11) (2012) 4162–4172.

[32] Y.J. No, S.I. Roohani-Esfahani, Z. Lu, T. Schaer, H. Zreiqat, Injectable radiopaque and bioactive polycaprolactone-ceramic composites for orthopedic augmentation, J. Biomed. Mater. Res. B Appl. Biomater. 103 (7) (2015) 1465–1477.

[33] E. Karamian, A. Nasehi, S. Saber-Samandari, A. Khandan, Fabrication of hydroxyapatite-baghdadite nanocomposite scaffolds coated by PCL/bioglass with polyurethane polymeric sponge technique, Nanomed. J. 4 (3) (2017) 177–183.

[34] H. Wang, Y. Li, Y. Zuo, J. Li, S. Ma, L. Cheng, Biocompatibility and osteogenesis of biomimetic nano-hydroxyapatite/polyamide composite scaffolds for bone tissue engineering, Biomaterials 28 (22) (2007) 3338–3348.

[35] S. Das, S.J. Hollister, C. Flanagan, A. Adewunmi, K. Bark, C. Chen, K. Ramaswamy, D. Rose, E. Widjaja, Freeform fabrication of Nylon-6 tissue engineering scaffolds, Rapid Prototyp. J. 9 (1) (2003) 43–49.

[36] R. Nirmala, R. Navamathavan, H.-S. Kang, M.H. El-Newehy, H.Y. Kim, Preparation of polyamide-6/chitosan composite nanofibers by a single solvent system via electrospinning for biomedical applications, Colloids Surf. B: Biointerfaces 83 (1) (2011) 173–178.

[37] J. Shen, Y. Li, Y. Zuo, Q. Zou, L. Cheng, L. Zhang, M. Gong, S. Gao, Characterization and cytocompatibility of biphasic calcium phosphate/polyamide 6 scaffolds for bone regeneration, J. Biomed. Mater. Res. B Appl. Biomater. 95 (2) (2010) 330–338.

[38] A. Abdal-hay, K.A. Khalil, F.F. Al-Jassir, A.M. Gamal-Eldeen, Biocompatibility properties of polyamide 6/PCL blends composite textile scaffold using EA. hy926 human endothelial cells, Biomed. Mater. 12 (3) (2017) 35002.

[39] A. Abdal-hay, Y.S. Oh, A. Yousef, H.R. Pant, P. Vanegas, J.K. Lim, In vitro deposition of Ca-P nanoparticles on air jet spinning nylon 6 nanofibers scaffold for bone tissue engineering, Appl. Surf. Sci. 307 (2014) 69–76.

[40] A. Abdal-hay, A.S. Hamdy, Y. Morsi, K.A. Khalil, J.H. Lim, Novel bone regeneration matrix for next-generation biomaterial using a vertical array of carbonated hydroxyapatite nanoplates coated onto electrospun nylon 6 nanofibers, Mater. Lett. 137 (2014) 378–381.

[41] S. Cakir, R. Kierkels, C. Koning, Polyamide 6-polycaprolactone multiblock copolymers: synthesis, characterization, and degradation, J. Polym. Sci. A Polym. Chem. 49 (13) (2011) 2823–2833.

[42] A. Monshi, M.R. Foroughi, M.R. Monshi, Modified Scherrer equation to estimate more accurately nano-crystallite size using XRD, World J. Nano Sci. Eng. 2 (3) (2012) 154–160.

[43] N.O. Engin, A.C. Tas, Manufacture of macroporous calcium hydroxyapatite bioceramics, J. Eur. Ceram. Soc. 19 (13–14) (1999) 2569–2572.

[44] M. Bohner, J. Lemaitre, Can bioactivity be tested in vitro with SBF solution? Biomaterials 30 (12) (2009) 2175–2179.

[45] M. Yazdimamaghani, D. Vashaee, S. Assefa, K. Walker, S. Madihally, G. Köhler, L. Tayebi, Hybrid macroporous gelatin/bioactive-glass/nanosilver scaffolds with controlled degradation behavior and antimicrobial activity for bone tissue engineering, J. Biomed. Nanotechnol. 10 (6) (2014) 911–931.

[46] N. Golafshan, M. Kharaziha, M. Fathi, Tough and conductive hybrid graphene-PVA: alginate fibrous scaffolds for engineering neural construct, Carbon 111 (2017) 752–763.

[47] S. Sadeghpour, A. Amirjani, M. Hafezi, A. Zamanian, Fabrication of a novel nanostructured calcium zirconium silicate scaffolds prepared by a freeze-casting method for bone tissue engineering, Ceram. Int. 40 (10) (2014) 16107–16114.

[48] A. Najafinezhad, M. Abdellahi, H. Ghayour, A. Soheily, A. Chami, A. Khandan, A comparative study on the synthesis mechanism, bioactivity and mechanical properties of three silicate bioceramics, Mater. Sci. Eng. C 72 (2017) 259–267.

[49] M. Sukul, Y.-K. Min, B.-T. Lee, Collagen-hydroxyapatite coated unprocessed cuttlefish bone as a bone substitute, Mater. Lett. 181 (2016) 156–160.

[50] Z. Nan, Z. Shi, B. Yan, R. Guo, W. Hou, A novel morphology of aragonite and an abnormal polymorph transformation from calcite to aragonite with PAM and CTAB as additives, J. Colloid Interface Sci. 317 (1) (2008) 77–82.

[51] H.-H. Jin, C.-H. Lee, W.-K. Lee, J.-K. Lee, H.-C. Park, S.-Y. Yoon, In-situ formation of the hydroxyapatite/chitosan-alginate composite scaffolds, Mater. Lett. 62 (10 − 11) (2008) 1630–1633.

[52] I. Sabree, J. Gough, B. Derby, Mechanical properties of porous ceramic scaffolds: influence of internal dimensions, Ceram. Int. 41 (7) (2015) 8425–8432.

[53] M. Diba, M. Fathi, M. Kharaziha, Novel forsterite/polycaprolactone nanocomposite scaffold for tissue engineering applications, Mater. Lett. 65 (12) (2011) 1931–1934.

[54] S. Zhou, L. Zhang, Y.-Y. Wang, Y. Zuo, S.-B. Gao, Y.-B. Li, Fabrication of hydroxyapatite/ethylene-vinyl acetate/polyamide 66 composite scaffolds by the injection-molding method, Polym.-Plast. Technol. Eng. 50 (10) (2011) 1047–1054.

[55] M.-Z. Yao, M.-Y. Huang-Fu, H.-N. Liu, X.-R. Wang, X. Sheng, J.-Q. Gao, Fabrication and characterization of drug-loaded nano-hydroxyapatite/polyamide 66 scaffolds modified with carbon nanotubes and silk fibroin, Int. J. Nanomedicine 11 (2016) 6181.

[56] G. Gurato, A. Fichera, F.Z. Grandi, R. Zannetti, P. Canal, Crystallinity and polymorphism of 6-polyamide, Die Makromolekulare Chemie: Macromolecular Chemistry and Physics 175 (3) (1974) 953–975.

[57] J. Wei, Y. Li, K.-T. Lau, Preparation and characterization of a nano apatite/polyamide6 bioactive composite, Compos. Part B 38 (3) (2007) 301–305.

[58] X. Zhang, M. Lu, Y. Wang, X. Su, X. Zhang, The development of biomimetic spherical hydroxyapatite/polyamide 66 biocomposites as bone repair materials, Int. J. Polym. Sci. 2014 (2014).

[59] K. Pramoda, T. Liu, Z. Liu, C. He, H.-J. Sue, Thermal degradation behavior of polyamide 6/clay nanocomposites, Polym. Degrad. Stab. 81 (1) (2003) 47–56.

[60] W. Jie, L. Yubao, Tissue engineering scaffold material of nano-apatite crystals and polyamide composite, Eur. Polym. J. 40 (3) (2004) 509–515.

[61] L. Gibson, Mechanical behavior of metallic foams, Annu. Rev. Mater. Sci. 30 (1) (2000) 191–227.

[62] A. Abdal-hay, H.R. Pant, J.K. Lim, Super-hydrophilic electrospun nylon-6/hydroxyapatite membrane for bone tissue engineering, Eur. Polym. J. 49 (6) (2013) 1314–1321.

[63] H. Li, J. Chang, Fabrication and characterization of bioactive wollastonite/PHBV composite scaffolds, Biomaterials 25 (24) (2004) 5473–5480.

[64] S. Ramezani, R. Emadi, M. Kharaziha, F. Tavangarian, Synthesis, characterization and in vitro behavior of nanostructured diopside/biphasic calcium phosphate scaffolds, Mater. Chem. Phys. 186 (2017) 415–425.

[65] X. Qian, F. Yuan, Z. Zhimin, M. Anchun, Dynamic perfusion bioreactor system for 3D culture of rat bone marrow mesenchymal stem cells on nanohydroxyapatite/polyamide 66 scaffold in vitro, J. Biomed. Mater. Res. B Appl. Biomater. 101 (6) (2013) 893–901.

[66] F. Pahlevanzadeh, H.R. Bakhsheshi-Rad, A.F. Ismail, M. Aziz, Apatite-forming ability, cytocompatibility and mechanical properties enhancement of PMMA-based bone cements by incorporating of baghdadite nanoparticles, Int. J. Appl. Ceram. Technol..